OPEN leaf: an open-source cloud-based phenotyping system for tracking dynamic changes at leaf-specific resolution in Arabidopsis.

Landon G. Swartz[1,2], Suxing Liu[3], Drew Dahlquist[1], Skyler T. Kramer[4], Emily S. Walter[2], Samuel A. McInturf[2], Alexander Bucksch[3], David G. Mendoza-Cózatl[1,2,*]

[1]Department of Electrical Engineering and Computer Science, University of Missouri-Columbia, USA.
[2]Division of Plant Science and Technology, C.S. Bond Life Sciences Center, University of Missouri, Columbia, USA.
[3]School of Plant Sciences, University of Arizona, Tucson, USA.
[4]MU Institute of Data Science and Informatics, University of Missouri-Columbia, USA.

Short title: Leaf-specific tracking and phenotyping.

Keywords: CyVerse, high-throughput phenotyping, hydroponics, phenomics, plant nutrition.

Corresponding author:

D. G. Mendoza-Cózatl
Division of Plant Sciences and Technology,
C.S. Bond-Life Sciences Center.
University of Missouri, Columbia
1201 Rollins Street (271F)
Columbia, MO 65211, U.S.A.
Phone: (+1) 573-882 1892
Email: mendozad@missouri.edu

Abstract:

The first draft of the *Arabidopsis* genome was released more than 20 years ago and despite intensive molecular research, more than 30% of *Arabidopsis* genes remained uncharacterized or without an assigned function. This is in part due to gene redundancy within gene families or the essential nature of genes, where their deletion results in lethality (*i.e.,* the *dark genome*).

High-throughput plant phenotyping (HTPP) offers an automated and unbiased approach to characterize subtle or transient phenotypes resulting from gene redundancy or inducible gene silencing; however, access to commercial HTPP platforms remains limited. Here we describe the design and implementation of *OPEN leaf*, an open-source phenotyping system with cloud connectivity and remote bilateral communication to facilitate data collection, sharing and processing.

OPEN leaf, coupled with our SMART imaging processing pipeline was able to consistently document and quantify dynamic changes at the whole rosette level and leaf-specific resolution when plants experienced changes in nutrient availability. Our data also demonstrate that VIS sensors remain underutilized and can be used in high-throughput screens to identify and characterize previously unidentified phenotypes in a leaf-specific time-dependent manner. Moreover, the modular and open-source design of *OPEN leaf* allows seamless integration of additional sensors based on users and experimental needs.

Significance Statement

Many bottlenecks still exist in the high-throughput plant phenotyping (HTPP) field, including open access to algorithms, computing power for image processing, and a limited access to affordable HTPP platforms. Closing the genome-to-phenome gap requires more accessible open-source and accessible HTPP options; hence, we developed an affordable open-source top-view automated phenotyping system that allows the quantification of traits at a whole rosette and leaf-specific resolution.

Introduction

Understanding genome-to-phenome relationships is at the core of *predictive biology*, whose aim is to predict a biological outcome from a known input (Lopatkin & Collins, 2020). The phenome, however, is also the result of specific environmental conditions and the ability of organisms to sense and adapt to changes in their environment (Des Marais *et al.*, 2013; Xu, 2016; Buckner *et al.*, 2019). Thus, *predictive biology* requires deep mechanistic understanding of the genetic makeup of a given organism but also its plastic response to environmental cues. In the case of plants, these cues may include changes in light intensity, nutrient, and water availability, and the presence of other organisms, including microbes or additional plant species (Lundberg *et al.*, 2012; Legris *et al.*, 2016). While significant advances have been made to understand plant behavior at the molecular, physiological, and ecological level, the prediction of plant responses during changing environments remains a formidable challenge that requires consistent collection of reproducible data at the "*-omic*" and environmental levels.

Collecting large amounts of genomic and environmental data have become reasonably affordable in recent years; however, integrating, sharing, and analyzing such data in real-time is currently a bottleneck in biology. Moreover, the methods for characterizing genomes and phenomes have not advanced at the same rate (Moore *et al.*, 2013; Yang *et al.*, 2020). While genomic techniques have benefited from new developments in DNA sequencing, including higher resolution and lower costs, plant phenotyping has improved at a slower rate and commercial plant phenotyping platforms remained costly and practically inaccessible for purchase by the majority of plant laboratories (Shendure & Ji, 2008; Jackson *et al.*, 2011; White *et al.*, 2012; Reynolds *et al.*, 2019). More importantly, this gap between genomic and phenomic technologies are preventing the full use of resources available in several plant species such as mutant collections or diversity panels to pursue genome-wide studies or the characterization of complex traits at a higher resolution (Xiao *et al.*, 2017). At the same time, the technology needed for high-throughput plant phenotyping studies including sensors, computer vision, and information technology (IT), have become more accessible, allowing the development of diverse platforms for plant phenotyping experiments including roots (Le Marié *et al.*, 2014; Mathieu *et al.*, 2015), shoots (Awlia *et al.*, 2016; Flood *et al.*, 2016), plant growth within laboratory or greenhouse spaces (van der Heijden *et al.*, 2012; Yang *et al.*, 2014) and large field crops (Sadeghi-Tehran *et al.*, 2017; Maes & Steppe, 2019). In addition to biological insights, these platforms have also identified three major limitations in high-throughput plant phenotyping (HTPP) platforms, that is: (i) the ability to consistently reproduce abiotic stresses such as water and nutrient limitation (ii) data management that is standardized and comprehensive for collaborative analysis and re-analysis (iii) and the high cost of commercial high-throughput phenotyping platforms (Billiau *et al.*, 2012; Tsaftaris & Scharr, 2019; Reynolds *et al.*, 2019; Yang *et al.*, 2020).

Here we describe *OPEN leaf* [Open PhENotyper for *leaf* **tracking**], an open-source plant phenotyping platform designed to track growth and development of rosette leaves in a leaf-specific manner. Our system was built considering accessible materials worldwide and it is primarily based on a high-resolution camera hovering over user-defined positions to track the morphology (size, shape, color) of the whole rosette and specific leaves. As a semi-autonomous platform, *OPEN leaf* is enabled to communicate remotely with users on a user-defined basis to track data in real-time, thus allowing adjustments throughout the experiments. *OPEN leaf* was developed to be modular, scalable, and includes cloud-based capabilities for data sharing and processing. As a proof-of-concept, here we describe the use of *OPEN leaf* to characterize *Arabidopsis* plants grown hydroponically with different nutrient levels. Reproducibility in the field of plant nutrition is a major roadblock, particularly in micronutrient deficiency studies, where the absolute concentration of elements in the nutrient solution and their ratio with other micronutrients have profound effects on day-to-day phenotypes (Nguyen *et al.*, 2016). With its cloud-based capabilities enabled, *OPEN leaf* was able to resolve dynamic phenotypes in a leaf-specific resolution during changes iron/zinc ratios. Our results demonstrate that within the *Arabidopsis* rosette, multiple phenotypes remain to be identified and that clear developmental changes occur in parallel to the standard chlorosis induced by iron deficiency.

Materials and Methods

Hardware

OPEN leaf was built using the open-source T-slot aluminum beams from 80/20 (https://8020.net) and a C-Beam Linear Actuator Bundle from OpenBuilds, which contains the track, a gantry plate, and a NEMA23 stepper motor (https://openbuildspartstore.com/c-beam-linear-actuator-bundle/). A high-resolution camera (Allied Vision Mako G-503) was mounted on the gantry plate using a bracket 3D printed on a Prusa i3 MK3 (STL file provided in Supp data; https://www.prusa3d.com). The track system moves to eight pre-determined positions using GRBL, an open-source, embedded, and high-performance g-code parser controlled by an Arduino microcontroller (https://www.arduino.cc). For a detailed bill of materials, 3D files, schematics and assembly manual see *Supplementary data*.

Software

OPEN *leaf* is controlled by an open-source desktop application written in C# (*OPEN Controller*, github.com/DMendozaLab/OPEN-Controller), and allows multi-machine control. From the desktop application, the user can identify and select the proper controller (machine) and its unique camera, or other sensors associated with it. The user also selects pre-defined camera settings including gain and aperture, the folder where the pictures will be saved and the GRBL commands to move the gantry plate with the camera attached to specified locations on the track. At each specific location, the camera will take a picture at one time point or a time series for a period of time defined by the user. Installation of *OPEN Controller* is streamlined by a package (*i.e.,* installer), which downloads and compiles all the required dependencies.

Cloud Integration

Integration for CyVerse (https://CyVerse.org) is an optional module of the OPEN series of devices that will send data to CyVerse for cloud storage, access, management, sharing, and analysis. CyVerse integration is done through the desktop application Cyberduck and a command-line interface (CLI) that interacts with CyVerse. Using CyVerse configuration profiles, one can log into a desired CyVerse account to have remote access to a respective CyVerse Data Store. For automated syncing (uploading), we created a python script titled *cyverse.py* that runs a duck -synchronize command to synchronize all data in the local directory to the remote directory located on CyVerse.

Slack Integration

We used the Slack tool called "bot" account to relay messages regarding the operational status of our OPEN machines. The "bot" account is setup onto a desired channel within a Slack teamspace with the proper permissions. Instructions to integrate Slack with OPEN machines can be found on (github.com/DMendozaLab/OPEN-leaf-cloud). For messages, we first query whether the phenotyping machine is currently running or not. If the machine is running then a message of "Status: Running" is sent with the current experiment name, and the latest single cycle images are sent. If the machine is not running, then a message of "Status: Dormant" is sent. After seven dormant messages are sent, no more dormant messages are sent until a new experiment is started and the status is updated to "Running". The status of the machine can be scheduled at specific times per day or "on demand" using slash commands (*e.g.,* /srp-get-status).

Image processing using *SMART*

SMART (Speedy Measurement of Arabidopsis Rosette Traits) is a complete set of parameter-free pipeline to analyze plant images in the visible (VIS) and near-infrared spectrum (NIR). The SMART pipeline use top-view images of *Arabidopsis* to compute geometrical traits of the whole rosette and if desired, SMART can also extract information from individual leaves in within the rosette (Table 1). For plant object segmentation and unlike other plant image pipelines that use a threshold value in color space, SMART uses a dominant color clustering method to segment the plant object from the background. The pipeline used are available as source code on GitHub (https://github.com/Computational-Plant-

Science/SMART) and are also available as a prepackaged Docker container (https://hub.docker.com/r/computationalplantscience/smart). For the identification and characterization of individual leaves and their corresponding parameters, SMART adopted a watershed segmentation algorithm. This algorithm first uses Euclidean Distance Transform to compute the Euclidean distance map to the closest zero (*i.e.,* background pixel) for each of the foreground pixels. Then each peak in the Euclidean distance map was fed as the markers for watershed segmentation to segment and count each of the plant leaves (van der Walt *et al.*, 2014). In addition, SMART was able to compute the color distribution and recognize distinct shades of color on the plant leaf surface.

Plant growth conditions

Arabidopsis Col-0 seeds were surfaced sterilized and geminated on 1/4 Murashige and Skoog (MS) medium after stratification for 2-4 days at 4°C in the dark. Then, seeds were allowed to germinate under 16 h light/ 8h dark cycles, 23°C day/ 21°C night (60 % humidity) as previously described (Nguyen *et al.*, 2016). After the emerging of the first true leaves (10-12 days after seed plating), plants were transferred to black magenta boxes using 3D printed floaters (See Supp data for STL files). Unless otherwise stated, plants were maintained in standard Arabidopsis hydroponic media as described in Nguyen et al. (2016) and imaged every four hours using the *OPEN leaf* system described here. Hydroponic media were saturated with air using standard aquarium air pumps and bubbling stones and the nutrient solution was changed every three days. After 4-6 days of continuous image capturing, the nutrient solution of some plants was replaced with hydroponic without Fe or with hydroponic media containing 15 μM Zn with and without Fe (the standard solution contained 5 μM Zn and 20 μM Fe).

Phytohormone measurements

Fresh rosette leaves from control plants and Fe deficient plants were flash frozen and stored at -80 C until processing by the Metabolomics core at the University of Missouri. Liquid nitrogen was used to grind the tissue to a final powder, and samples were kept frozen at all times before extraction. 100 mg of each sample was weighed into a glass vial and 1 ml of extraction solvent (Isopropanol:Water:HCl 2:1:0.002) was added along with 50 uL of internal standard solution (0.25 ug/mL of trans zeatin-d5, castasterone-d3, salicylic acid-d4, indole-3-acetic acid-d2, jasmonic acid-d5, abscisic acid-d6 and gibberellin A4-d2). Samples were shaken for 1 hour at 4 C, then 500 uL of dichloromethane was added to each sample followed by an additional 30 min of shaking at 4 C. Samples were then centrifuged at 3500 *g* for 20 min after which 2 phases are apparent. 800 uL of the bottom layer was transferred to an autosampler vial and completely dried down using a nitrogen dryer taking care not to overdry, as volatile components could be lost. Samples were reconstituted in 100 uL of methanol, then 1 mL of 1 % acetic acid was added.

Samples were then purified by solid phase extraction using Oasis HLB 1cc (30 mg) extraction cartridges (Waters, Inc.). After eluting samples from the SPE cartridges, samples were completely dried down. Samples were reconstituted in 25uL of methanol, then 25uL of 1% acetic acid was added. The samples were transferred to limited volume inserts and analyzed on a Waters Acquity UHPLC system coupled to a Waters Xevo TQ-XS mass spectrometer. Separation of phytohormones was achieved on a Waters Acquity 2.1 x 150 mm, 1.7 µm UPLC BEH C18 column using the following 25 min gradient: mobile phase B (acetonitrile) increased from 5% to 46% over 19 min, then to 90% in 0.1 min, held at 90% for 2 min, and returned to 95% mobile phase A (0.1% formic acid in water) for equilibration for 4 min. Sample injections were 2 uL, flow rate was 0.4 mL/min and column temperature was 40 C. Mass Spectrometry data was acquired using multiple reaction monitoring (MRM) and the transitions for each phytohormone can be found in Supplementary Table 1.

Elemental analysis

Elemental composition of source and sink leaves was determined by Inductively coupled plasma - optical emission spectrometry (ICP-OES) as previously described in Chen *et al.* (2006). Briefly, young and mature leaves were collected separately at the end of the phenotyping experiments, 1 week after treatment, and rinsed with Milli-Q water. Samples then were washed once with Tris 20 mM, EDTA 5 mM, pH 8.0 to eliminate ions bound to the surface and rinsed again with water. Samples were then dried, weighed, and digested using HNO_3 70 %. After digestion samples were diluted in Milli-Q water to 10 mL and analyzed for transition elements composition by ICP-OES. When needed leaves were separated according to its age as previously described (Nguyen et al., 2022). Briefly, mature leaves are leaves that developed since the early vegetative stage of the plants and had trichomes far apart on the leaf surface while young leaves were closer to the rosette's central top.

Statistical analysis

The SMART pipeline data is outputted as a command separated values file. Visualizations and statistics were done using the R programming language and related data science packages, including tidyverse, rstatix, and ggpubr (Wickham *et al.*, 2019). For figures 3-6, visualizations display the mean of the computed trait with standard error as the confidence intervals. Rstatix provides simple and intuitive pipe-friendly framework for performing statistical tests. Welch's t-test, an adaptation of Student's t-test that is more reliable when two samples have unequal variance, were conducted on Table 2 and Supplemental Table 2 from the rstatix R package for the whole rosette leaf area in pixels. Significance was determined with a p-value ≤ 0.05. A repeated measures ANOVA test was conducted in Supplemental Table 3 on manually selected clusters by age leaves to determine significance in relation to leaf area in pixels from the SMART pipeline.

Results

OPEN leaf design

High-throughput plant phenotyping (HTPP) has revolutionized the way plant scientists gather, process and extract information from plants, including model and crop species. However, commercial HTPP devices remain exceptionally expensive for laboratories around the world. Alternatively, several open-source HTPP devices are now available, but their assembly and operation still require a high degree of proficiency in mechanical engineering or computer sciences. To address this issue, we designed a top-view single row phenotyper (*OPEN leaf*; Figure 1A). We streamlined the assembly of *OPEN leaf* by taking advantage of affordable pre-assembled tracks available worldwide combined with controllers and open-source software (Figure 1B). At the core of *OPEN leaf* is a high-resolution camera that captures images suitable to be processed with current computer vision pipelines. In addition, we took advantage of CyVerse, a publicly accessible cyberinfrastructure, and Slack, a team communication platform, to enable cloud-storage, data sharing and processing, and a two-way communication protocol to remotely request operational status and data from *OPEN leaf* on a regularly basis or on-demand (Figure 1C).

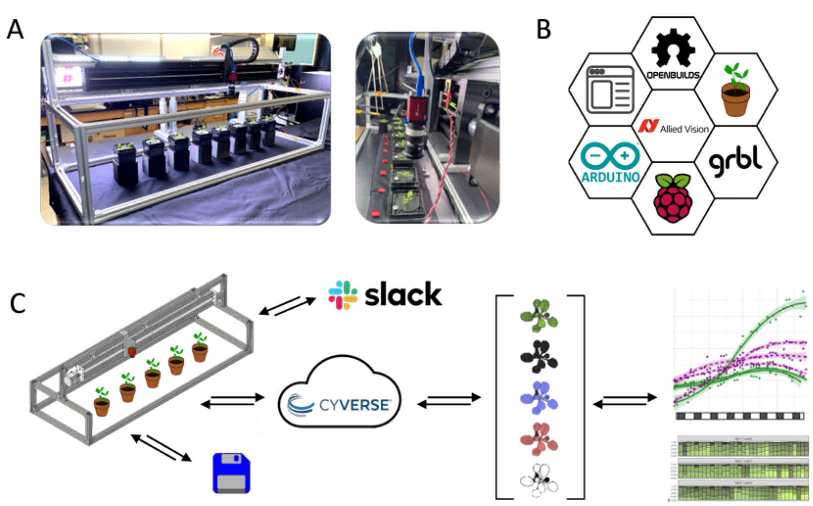

Figure 1 *OPEN leaf* design and capabilities. (a) The main components of the OPEN *leaf* imaging system are aluminum extrusion beans, a linear actuator and a high-resolution VIS camera to capture top-view

images of Arabidopsis plants grown hydroponically at eight independent positions. (b) The software and hardware required to operate OPEN *leaf* is based on publicly available packages and materials available worldwide. (c) To facilitate data sharing management, we have included optional cloud-based connectivity for remote data sharing processing and real-time operational status updates initiated on-demand by the end user.

OPEN leaf user interface and remote connectivity

The *OPEN leaf* user interface (*OPEN controller*) was designed so users can easily identify the critical parts of the system (*i.e.,* camera, storage path, and coordinates to stop along the track; Figure 2A) and have a one-stop access to modify each of them as needed. *OPEN controller* also allows users to capture images at one time point (single cycle) or over a user-defined period of time (time lapse). Images are initially stored locally in a hard drive, but we have also taken advantage of the publicly available cloud cyberinfrastructure CyVerse and its *Discovery Environment* to upload images regularly and facilitate data sharing and processing (scripts available in Supplementary Data). To further engage remote access and communication with *OPEN leaf,* we implemented a two-way communication using Slack (Figure 2B, scripts also available in Supplementary Data). This remote communication allows regularly updates on the operational status of the machine together with the last set of images taken when an experiment is ongoing. Alternatively, if the machine has finished the required cycles or the machine has stopped working due to a power interruption or computer malfunction the user will receive “dormant” status at the specified time (Figure 2B-C). Operational status can also be requested on demand with a similar outcome: “running + experiment + data” or “dormant” (Figure 2D-E).

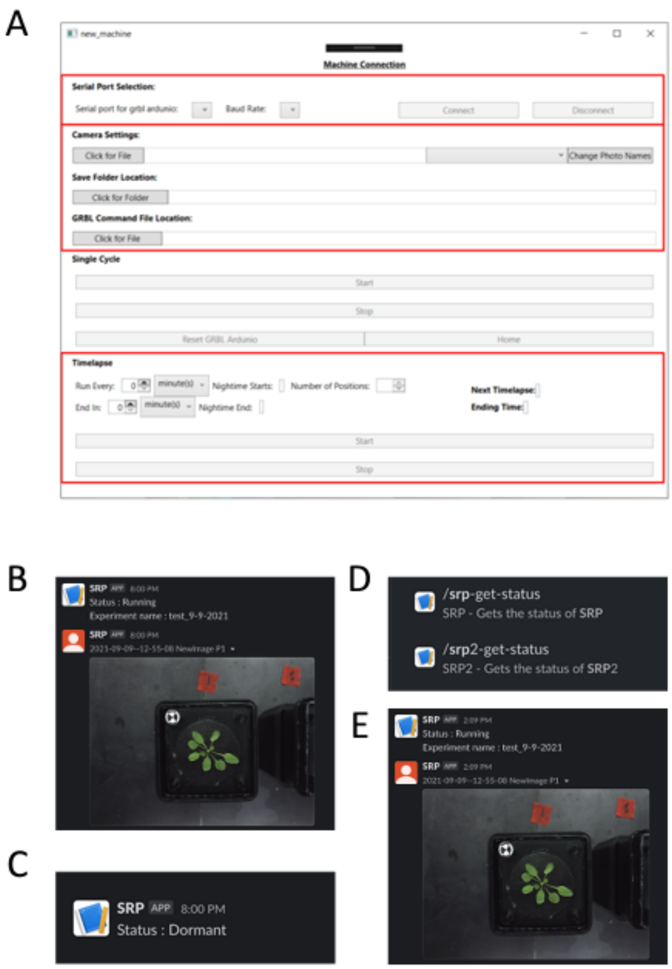

Figure 2 *OPEN* leaf user interface and remote communication. (a) The OPEN *leaf* user-interface was designed to be linear and intuitive with one-to-one relationships to control the different settings of the imaging system. (b-c) The use of the communication platform Slack, allow users can receive automatic updates of ongoing experiments indicating the status of the machine and the latest acquired data. (d-e) In addition, users can request on-demand updates for independent machines running simultaneously.

Feature extraction of rosette leaves using SMART

To begin testing the capabilities of *OPEN leaf* and the SMART image processing package, we first tracked the growth of *Arabidopsis* rosettes grown hydroponically in replete media or lacking Fe for 7 days. In these experiments, plants were first germinated on agar plates for 7-10 days before being transferred to magenta boxes with replete nutrient solution. After two days of acclimation in the hydroponic system, plants were placed under the *OPEN leaf* track and imaged continuously for two weeks. During the first week plants were grown in replete media to capture the baseline growth and after a week, half of the plants were grown on hydroponic media lacking Fe. While the experiment was running, images were uploaded to CyVerse and processed using the *Speedy Measurement of Arabidopsis Rosette Traits* (SMART) package (Figure 3A). SMART uses the top view of the *Arabidopsis* rosette to extract several geometrical traits of the whole rosette (Table 1). In contrast to other current processing pipelines, SMART is a parameter free algorithm that requires no human input of parameters before beginning the processing of images. Figure 3B shows an example of the automated rosette segmentation of plants grown in replete media or Fe deficiency. Only 11 representative images are shown but all the data points and traits, including color clustering, and the corresponding statistical analyses are available in Supplementary Table 2. Figure 3C shows the average area of the entire rosette of plants grown in the presence and absence of Fe and illustrates the negative impact that Fe deficiency has on growth and development, as well as the timing where these differences become statistically relevant (see also Table 2 for a subset comparison of whole rosette area within treatments). Note that the sensor used in these experiments was a visible image sensor (*i.e.*, a RGB color camera). As such, data collection was only possible during the light cycle of the imposed photoperiod (shown as open blocks on the *x* axis of Figure 3C). The selection of a visible image sensor was selected to maintain an affordable cost with the highest resolution possible that still allowed us to gain novel insights on the timing of Fe deficiency responses (see below); however, other sensors such as NIR cameras are compatible with the *OPEN leaf* track system and the SMART imaging software. To better understand the mechanistic basis of the growth delay observed in Arabidopsis rosettes experiencing Fe limitation, we measured the levels of the main 7 phytohormones in plants subjected to Fe deficiency for 24 and 48 hrs. These analyses showed minor changes in the phytohormone levels after 24 hrs of Fe deficiency; however, after 48 hrs of Fe deprivation, levels of auxin (IAA), gibberellins (GA_4), and cytokinin (trans-Zeatin), dropped significantly compared to control plants (Figure 3D). These results provide a physiological basis to explain the growth delay observed in plants when Fe becomes limiting.

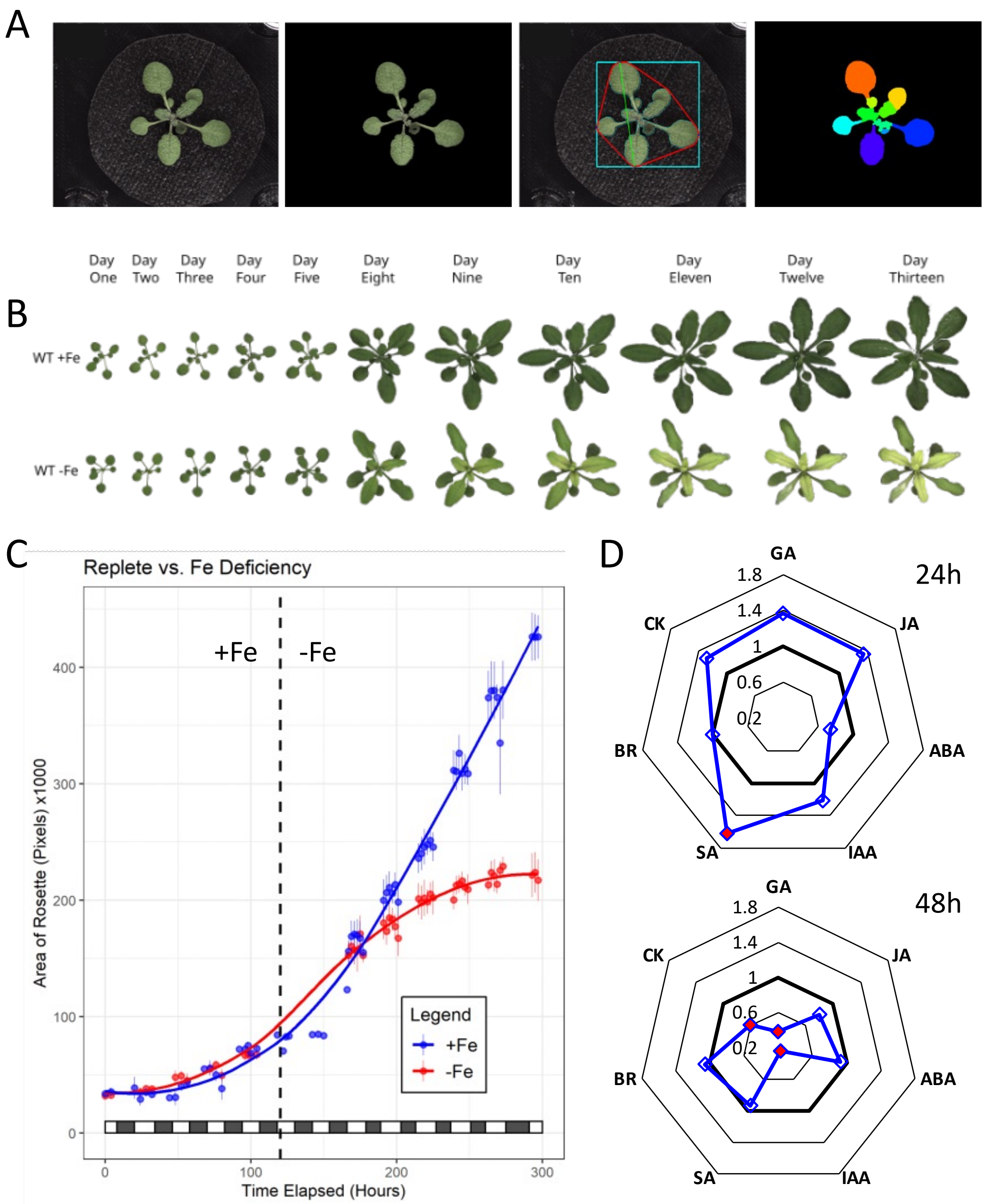

Figure 3 SMART imaging capabilities. (a) The *Speedy Measurement of Arabidopsis Rosette Traits* (SMART) is an automated pipeline to extract morphological information from Arabidopsis plants grown on the OPEN *leaf* imaging system, (b) the SMART pipeline can segment the Arabidopsis rosette and quantify several traits including leaf number, area and color [for a full list of traits see Table 1]. Day one refers to first day of imaging capture. (c) OPEN *leaf* and SMART are capable of detecting visual changes of Arabidopsis plants grown in the presence or absence of iron in the growth media, 5 µM Zn 20 µM Fe (+Fe), 5 µM Zn 0 µM Fe (-Fe). Each point represents the average of 4 individual plants per treatment ± SE (see Table 2 and Supplementary Table 2 for additional traits and the corresponding statistical analyses).

The white and black boxes at the bottom represent day and night. (d) Phytohormone levels in rosette leaves experiencing Fe deprivation for 24 and 48 hrs. Phytohormone levels are shown as a ratio between Fe deficient and sufficient plants and markers shown in red are statistically different from Fe sufficient plants ($p < 0.05$); quantitative data can be found in Supplementary Table 1.

Next, we tested whether our phenotyping platform was sensitive enough to detect changes when plants experience a combination of micronutrient availability. In these experiments, plants were grown hydroponically as described before but the nutrient challenge consisted in Fe deficiency experiments in the presence of standard zinc (Zn) concentrations (5 μM) or a mild elevated yet non-lethal concentration of Zn (15 μM) in the hydroponic solution. Figure 4A shows representative rosette images of each condition extracted using the SMART package and Figure 4B shows the area of the whole rosette plotted against time. Both, the images and the corresponding rosette, were able to capture differences in growth and development in each of the growth conditions. The addition of 15 μM Zn to the hydroponic media resulted in a smaller rosette area compared to plants grown with 5 μM Zn and these differences were more pronounced when Fe was removed from the media, particularly when plants were grown in 15 μM Zn. Also, while all treatments resulted in a small rosette size and chlorosis was only evident in plants experiencing Fe limitation, high Zn levels and Fe deprivation resulted in unique leaf colorations (darker green/purple) in source leaves at the bottom of the rosette (fully mature leaves). These results suggest that rosette growth as a whole and color in a leaf-specific manner contain traits that need to be analyzed and extracted independently (Figure 4B).

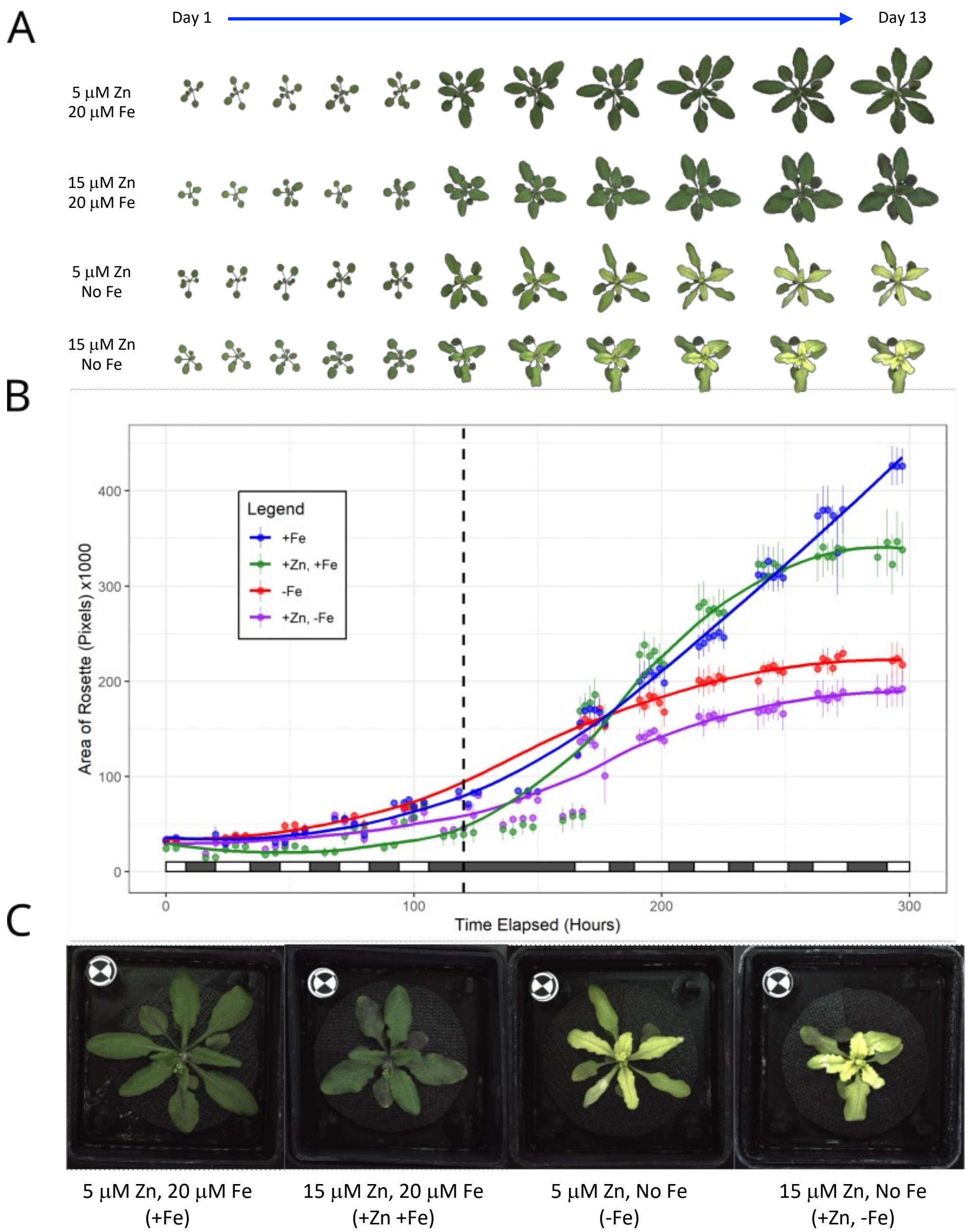

Figure 4 Arabidopsis phenotyping during contrasting changes in nutrient availability. (a) Whole rosette area and color are affected when iron (Fe) and zinc (Zn) were modified in the hydroponic media as indicated (b) the *OPEN leaf*-SMART pipeline was able to detect subtle changes in rosette when the Fe/Zn ratio was modified as follows: 5 µM Zn 20 µM Fe (+Fe), 15 µM Zn 20 µM Fe (+Zn +Fe), 5 µM Zn 0 µM Fe (-Fe), and 15 µM Zn 0 µM Fe (+Zn, -Fe). Each point represents the average of 4 individual plants per treatment ± SE (c) Changes in Fe and Zn lead to unique phenotypes in individual leaves within the entire rosette in a

pattern consistent with sink-source relationships. The white and black boxes at the bottom represent day and night, respectively. These experiments were repeated in triplicate with similar results.

SMART leaf-specific phenotyping

During the course of these experiments, we noticed that within treatments, the color of individual leaves within the *Arabidopsis* rosette changed substantially, in a manner consistent with source-sink relationships (Figure 4C). While these Fe-associated leaf-specific phenotypes have been described at the molecular level (Schuler *et al.*, 2012; Nguyen *et al.*, 2022), segmentation and quantification of visible traits in a leaf-specific manner is not standard in current phenotyping pipelines. Hence, we implemented a watershed segmentation algorithm to segment individual leaves within the *Arabidopsis* rosette (Figure 5). This watershed segmentation algorithm first uses *Euclidean Distance Transform* to calculate the Euclidean distance map to the closest zero (*i.e.*, background pixel) for each of the foreground pixels. In the following step, each peak in the Euclidean distance map was used as a marker for the watershed segmentation to identify and count each of the leaves within the rosette (Figure 5B). Once individual leaves were isolated, all different traits described for the full rosette were extracted including color using the dominant clustering method described before (Table 1; Supplementary Table 3, and Figure 5C-D).

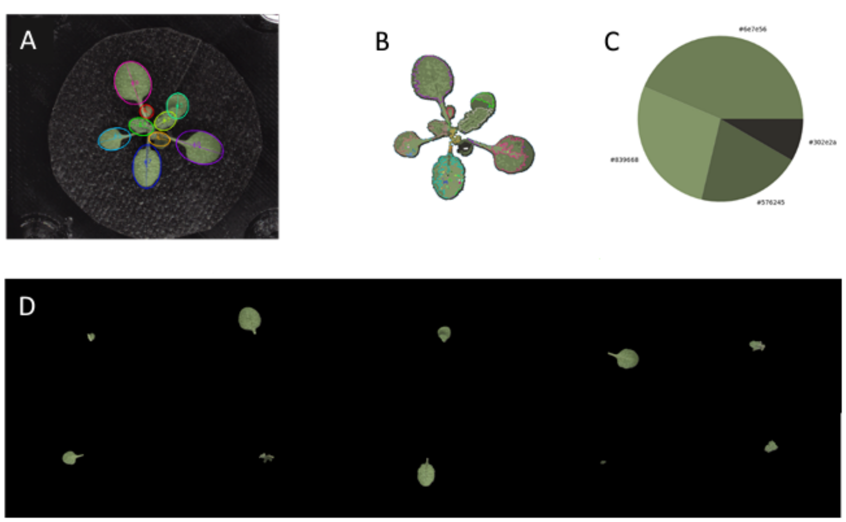

Figure 5 Leaf-specific segmentation of Arabidopsis rosette using SMART. (a-b) SMART is capable of segmenting individual leaves through watershed segmentation. (c-d) color is described as the top four dominant colors using hexadecimal values, and once the individual leaves have been identified and extracted, all the morphological traits described in Table 1 can be quantified in a leaf-specific manner.

To test the capabilities of our leaf-specific phenotyping approach, we compared plants grown in standard Zn levels (5 μM) plus Fe (5 μM Zn+Fe) with plants grown in 15 μM Zn without Fe (15 μM Zn-Fe). We chose these two conditions as starting point based on the data obtained using whole rosette phenotyping (Figure 4), where color changes in a leaf-specific manner were consistently observed. In turn, our individual leaf segmentation approach allowed us to classify individual rosette leaves in three main clusters (Figure 6). Cluster 1 represents the first true leaves within the rosette, whose area remain constant through the progression of the experiment; however, and as excepted for a *source* leaf, these leaves receive and retain the majority of micronutrients coming through the xylem stream and dictate the distribution of micronutrient across the rosette in a pattern consistent with their orthostichy (Khan *et al.*, 2018). Cluster 1 leaves show differences in leaf area at later times in the experiment but clear differences in color, particularly in plants grown with 15 μM Zn-Fe, which show hexadecimal color values consistent with darker green compared to the same leaves from plants grown in 5 μM Zn+Fe (Figure 6B and C). In contrast, Cluster 2 leaves represent individual leaves transitioning from sink (developing leaves) to source leaves (fully photosynthetic). In this cluster, the leaf area and color became more dependent on the environmental conditions (*i.e.*, nutrient availability) and their unique and autonomous developmental program. For instance, in 5 μM Zn+Fe, the leaf area of Cluster 2 leaves increased over time and their color remain constant through the entire experiment. However, growth of Cluster 2 leaves from plants grown in 15 μM Zn-Fe was variable, with some leaves being larger than control plants at the beginning of the treatment to later arrest growth at later stages (Figure 6B). Moreover, capturing color throughout the experiment allowed us to observe and quantify the transition of Cluster 2 leaves from dark green to yellow and this transition was consistent with the availability of high Zn and Fe at the beginning of the experiment to Fe deficiency in the later days of the experiment. (Figure 6C). Lastly, Cluster 3 leaves represent mostly *sink* leaves; thus, their appearance, color and size were more dependent on the nutrient availability. For instance, Cluster 3 leaves appearance was delayed in plants grown in 15 μM Zn-Fe compared to plants grown in 5 μM Zn+Fe (Figure 6A-B). Interestingly, Cluster 3 leaves from Fe deficient plants were consistently bigger in size than their counterpart in control plants and also were more chlorotic compared to leaves from plants grown in 5 μM Zn+Fe (Figure 6C). Altogether, these results demonstrate that *OPEN leaf* and SMART were able to capture the dynamic behavior of individual leaves within the *Arabidopsis* rosette when plants were exposed to different levels of nutrient availability.

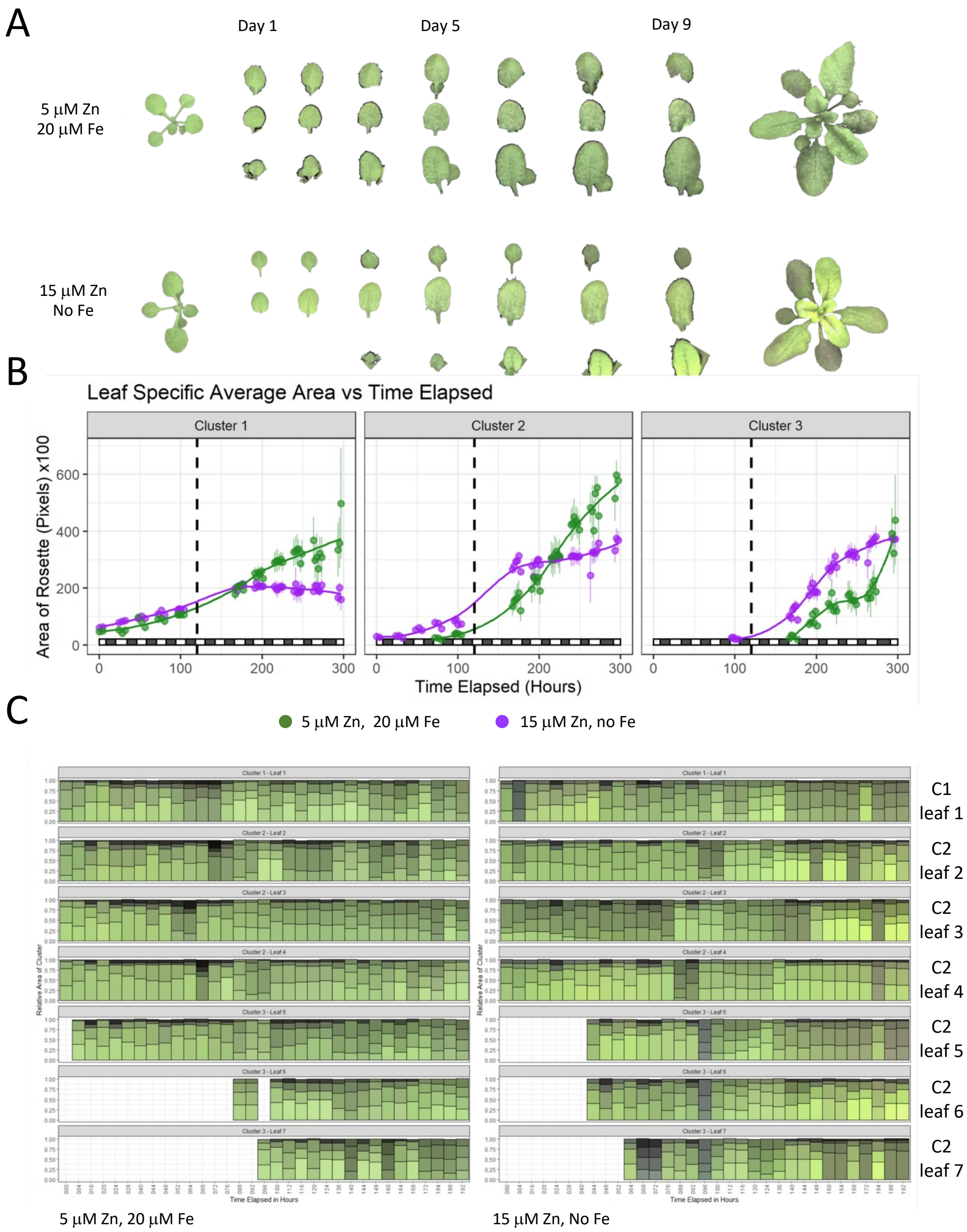

Figure 6 Nutrient availability dictates the fate of individual leaves within the Arabidopsis rosette. (a) the *OPEN leaf* – SMART pipeline is able to track individual leaves during plant growth and development. (b) Changes in the Fe/Zn ratio have a severe impact on individual leaf size and color and leaf clustering was consistent with the leaf developmental stage (source or sink). The white and black boxes at the bottom represent day and night, respectively. (c) Individual color clustering of the 4 dominant colors allows dynamic tracking of color transitioning during the entire experiment a at leaf-specific resolution. Each bar plot represents the proportional distribution of each dominant color in individual leaves from the clusters

shown in panel b. Cluster and leaf number are also shown on the right side of the right panel. The plots are representative of one experiment and similar results were obtained in three independent experiments.

While exploring different alternatives to visualize color changes in a 3D space, we found that this is an ongoing yet unresolved issue in the image processing and visualization field. This is because the RGB color space is an additive model that combines different numerical amounts (0 to 256) of the colors red, green, and blue for displaying color on a screen. Therefore, lighter colors such as chlorotic leaves are more difficult to visualize when plotted side-by-side with darker green leaves (Figure 7A)(Barten, 1999). Moreover, plotting the RGB values in normalized scale from contiguous images do not reflect the dynamic change between leaf clusters to the human eye (Figure 7B). Thus, we aimed to implement the 1976 CIELAB (or $L^*a^*b^*$) color space as defined by the International Commission on Illumination (International Commission on Illumination, 2007). In contrast to RGB, the CIELAB color space is device-independent and presents a three-dimensional representation of the entirety of the human visional range, which is more perceptually uniform than previous color space attempts. For instance, the L^* value closely matches human perception of the lightness of a color where 0 is defined as black and 100 as white, while the a^*b^* values represent red-green and yellow-blue color spectrums, respectively. The CIELAB space can also be represented in cylindrical form ($CIELCh_{ab}$) through simple transformation equations of the a^*b^* values within the *Colour* python package (Figure 7C) (Mansencal, Thomas *et al.*, 2022). This transformation of RGB colors is designed for better color display on monitors and by using this cylindrical model, we were able to better describe the color change trajectory of each of the leaf clusters through time.

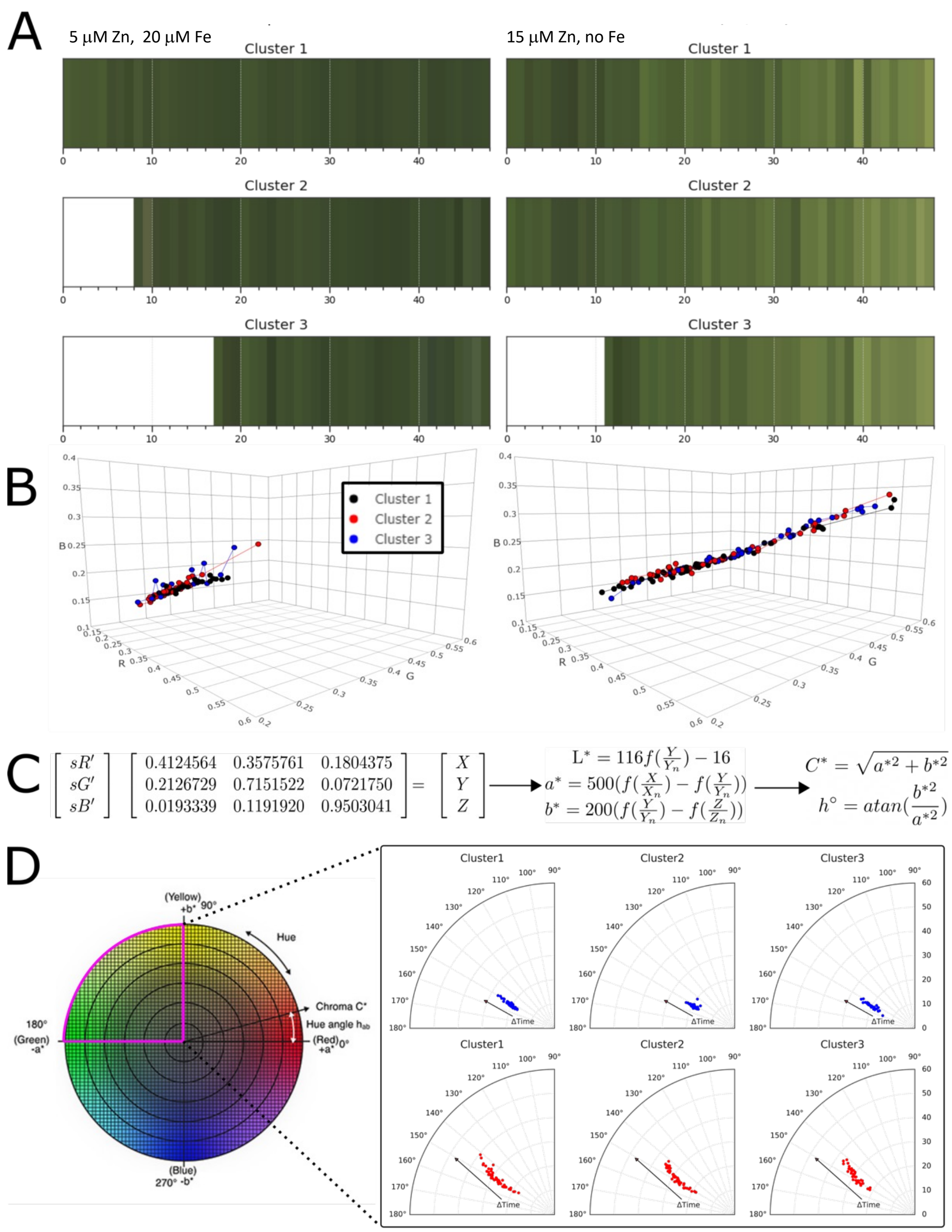

Figure 7 Most camera sensors capture images in standard RGB (sRGB) which is an additive model of color that takes the sum of red, green, and blue channels. (a) RGB values can show obvious changes in color from different colors but fails at displaying small changes in color visually even if it is numerical difference. (b) There are few ways to display the changes in sRGB values between clusters and between conditions (c) Converting sRGB to the tristimulus values of XYZ converts the additive model of RGB to something representing the human understanding of color. XYZ tristimulus values are converted to L*a*b* values via

standard conversion formulas and then to chroma and hue values. (d) The CIELChab model of colors can be graphed onto polar coordinates to show the distinct changes over time in colors to the cluster of leaves in a uniform manner.

One of the major advantages of image-based phenotyping is its non-destructive nature, which allows researchers to explore changes in visual phenotypes for long periods of time. However, end-point analytical measurements such as transcriptomics, proteomics, metabolomics, and ionomics, are also valuable as they provide absolute quantifiable values for traits of interest. Clearly, pairing each of the image-based phenotyping data points with analytical methods is not feasible; but conclusions offered by image-based phenotyping should be corroborated with end-point analytical approaches. To this end, we explored the *ionome* of plants experiencing changes in Fe availability under low and high Zn levels (Figures 4 and 6). To reduce data complexity, we focused on mature (source) and young (sink) leaves and conducted an elemental profiling of trace elements at the end of the visual phenotyping experiments (Figure 8). As expected, plants experiencing Fe limitation showed significant less Fe levels compared to plants grown in replete media regardless of the Zn content in the media. In addition, plants grown in replete media supplemented with 10 μM Zn also showed lower levels of Fe compared to plants grown in standard replete media containing 5 μM Zn, which is consistent with the fact that both Zn and Fe compete to enter the plant through the Iron-Regulated Transporter (IRT1) at the root level (Hindt & Guerinot, 2012). In turn, the levels of Zn increased in both mature and young leaves, which can be explained by the induction of *IRT1* during Fe limitation (Khan et al., 2018). Interestingly, the elemental profiling of young and mature leaves also revealed additional unique differences depending on Fe/Zn ratios. For instance, young leaves have significant higher levels K and Cu compared to mature leaves when plants experience Fe deficiency under standard Zn levels but during Zn excess, the levels of Cu and K in young levels are reduced suggesting that the ratio Fe/Zn impairs the metabolism of other ions in a leaf-specific manner and explains the leaf-specific differences observed through image-based phenotyping (Figure 6). Contrasting differences between source and sink leaves during nutritional deficiencies have been described before (García *et al.*, 2013; Nguyen *et al.*, 2022); but the precise mechanisms behind these differences are still elusive and require further investigation at the phenotypic, physiological, and molecular level.

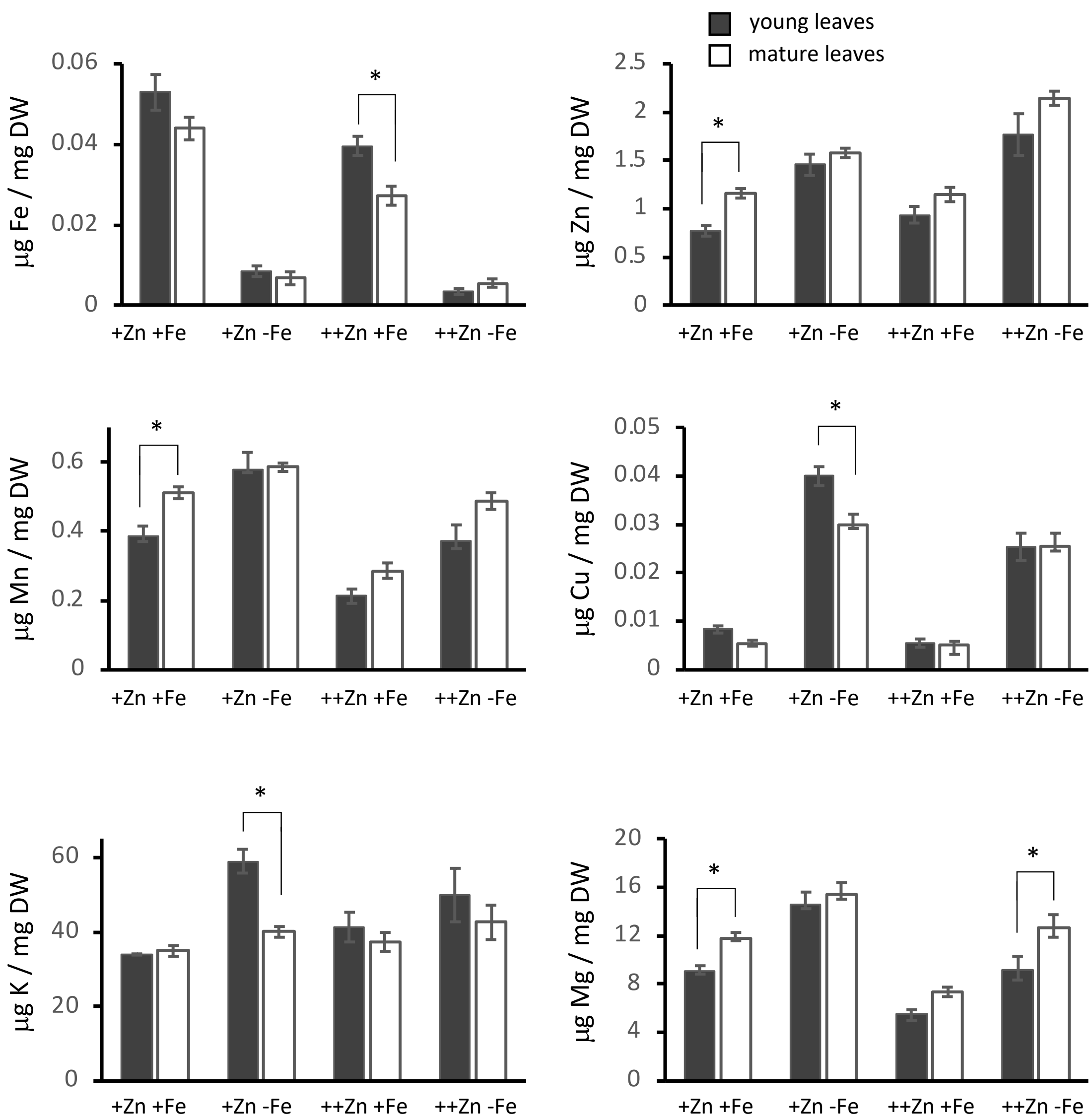

Figure 8 Elemental profiling of source and sink leaves experiencing iron limitation under different levels of zinc availability. Plants were grown under replete conditions (5 µM Zn, 20 µM Fe) for two weeks after being transplanted to hydroponics and then subjected to Fe deficiency under two different Zn availability conditions, standard [5 µM (+Zn)] or excess [15 µM (++Zn)], for one additional week. After the treatment, young (sink) and mature (source) leaves were identified as described previously (Nguyen *et al.*, 2022), collected, dried, and processed for elemental profiling. Only statistical differences between sink and source leaves are shown but comparisons across all treatments and statistical analyses can be found in Supplemental Table 4 and 5 (n = 4-5, mean ± S.E.).

Discussion

The Arabidopsis genome was released in the year 2000 and after more than two decades of intensive molecular research, 30% of its 25,000+ genes remain without an assigned function. Moreover, a greater number of genes in other species have been annotated based on homology without experimental evidence of their putative function (Wang *et al.*, 2019). There are many factors behind this gap in knowledge, including gene lethality or redundancy within gene families, which is not uncommon in higher plants. In addition, many mutations lead to subtle or transient phenotypes which are difficult to reproduce and capture with standard end-point documentation methods (*i.e.,* photos at the end of an experiment) or subject to experimental bias from environmental conditions or image processing protocols such as manual extraction of leaf traits including shape, size and color (Dobrescu *et al.*, 2017; Zhang *et al.*, 2020; Hernández-Herrera *et al.*, 2021).

High throughput plant phenotyping (HTPP) has emerged as a technology to solve many of these issues including consistency during data acquisition and processing (Acosta-Gamboa *et al.*, 2016; Vasseur *et al.*, 2018). HTPP has facilitated the discovery of novel genes and gene function through the use of large mutant collections and diversity panels or ecotypes (Campos *et al.*, 2021; Xie *et al.*, 2021). Unfortunately, commercial HTPP devices remain prohibitively expensive and thus are limited to the very few labs that can afford them. Fee-for-service HTPP facilities may be an affordable option for some labs as long as the HTPP facility is within reasonable distance or the appropriate logistics solutions are in place. Alternatively, many open-source HTPP devices have been published but their assembly and operation require significant expertise in mechanical engineering and computer science, which is not standard nor common in plant biology departments. However, a full and comprehensive characterization of genes with unknown function (i.e. the *dark genome*) requires a collective effort within the plant community. And at the core of this effort is accessibility to HTPP technologies, commercial or open-source, together with standard practices to conduct experiments under well-defined environmental conditions.

Here we described *OPEN leaf*, an open-source HTPP device with cloud connectivity and remote bilateral communication with users (Figures 1 and 2). *OPEN leaf* design is user-centered and takes advantage of affordable materials available worldwide, with an approximate cost of $1200 USD (as of Dec 2022; Manual assembly available in supplementary data). *OPEN leaf* together with the SMART processing suite offers a one-stop solution for HTPP of *Arabidopsis* rosettes, or other rosette-like plant species, from continuous and automatic data collection to data storage, sharing and processing. Our cloud integration approach solves one of the main issues in HTPP approaches, known as the FAIR principle for data management, where HTPP data should be findable, accessible, interoperable, and reusable for reasonable scientific advancement (Wilkinson *et al.*, 2016). The modular structure of *OPEN leaf* allows users to capture images at a user-defined frequency without the need for cloud or internet connectivity. This modularity also allows users to incorporate additional sensors such as NIR, fluorescence, multi- and hyperspectral cameras; however, each of these sensors will proportionally increase the cost of the HTPP device and data output.

In this work, we also aimed to demonstrate that, despite being one of the most basic sensors, visible cameras and RGB images, are still underutilized and several novel phenotypes occurring within the *Arabidopsis* rosette are yet to be identified, quantified, and characterized. For instance, rosette growth and development is known to be controlled by the intrinsic genetic program of the plant but can also be modified by environmental factors such as nutrient availability or the presence of pathogens (Hindt & Guerinot, 2012; Kim *et al.*, 2014). Our whole-rosette phenotyping pipeline was able to document the growth delay of plants experiencing Fe deficiency (Figure 3). Growth delay in Arabidopsis roots has been found to be mediated by the gibberellin pathway and the corresponding DELLA repressor proteins (Wild *et al.*, 2016). For instance, Arabidopsis plants lacking all DELLA proteins have longer roots during Fe deficiency compared to wildtype plants, suggesting that growth arrest during Fe deficiency is the result of proper Fe sensing followed by downstream hormone-developmental events but not the result of energy shortages due to impaired photosynthesis and respiration. Our phytohormone profiling in Arabidopsis leaves also suggest that Fe sensing and development is also tightly correlated as leaves experiencing Fe limitation show reduced levels of auxin, cytokinins, and gibberellins (Figure 3D). Notably, Fe sensing at the whole plant level is sensed in source leaves, which communicate the Fe status of the plant to roots *via* the phloem to either increase or repress Fe uptake at the root level (Khan *et al.*, 2018). It is therefore expected that a similar hormone-developmental signaling pathway associated with Fe sensing in leaves takes place but the molecular mechanisms behind Fe sensing in leaves remain largely unknown.

Hydroponic experiments over the last decades have provided a unique opportunity to explore plant responses to nutrient availability at a very high resolution and our *OPEN leaf*-SMART pipeline was able to capture subtle differences in rosette size and color during experiments were Fe and Zn availabilities were modified (Figure 4 and 5). Moreover, our phenotyping pipeline demonstrates that significant changes occur within the *Arabidopsis* rosette, in a leaf-specific manner, when the ratio of Fe/Zn availability changes (Figure 6). Leaf responses to nutrient availability are expected to be strikingly different from roots as the *Arabidopsis* rosette includes both sink and source tissues (*i.e.,* young and mature leaves), while roots are by definition a sink tissue. In fact, unique leaf-specific transcriptional responses have been described during Fe deficiency experiments in *Arabidopsis* where prolonged Fe deprivation leads to a restricted distribution of Fe to developing (sink) leaves to preserve optimal photosynthesis in mature (source) leaves (Hantzis *et al.*, 2018; McInturf *et al.*, 2022). While the precise molecular mechanisms behind Fe economy reprograming is ongoing, our *OPEN leaf*-SMART phenotyping pipeline was able to capture the timing of such leaf-specific changes, thus offering the sought-after time window to pursue additional molecular analyses to unravel the mechanisms behind plant responses and adaptation to nutrient availability in a leaf-specific manner.

Acknowledgments

This research was supported in part by the US National Science Foundation (MCB 2224839 and DEB 2217322), the MU Honors College and Peggy and Andrew Cherng Charitable Foundation (LS), the USDOE ARPA-E ROOTS (DE-AR0000821), the NSF CAREER Award No. 1845760 to A.B, and the US National Institute of Health BD2K Training Grant T32HG009060 grant (STK). We would also like to thank Wesley Paul Bonelli for his contribution to design the script collection data. Any opinions findings, and conclusions or recommendations expressed in this material are those of the author(s) and do not necessarily reflect those of ARPA-E or the National Science Foundation.

Conflict of Interest

The authors have no conflicts to declare.

Author Contribution

LGS, SM and DM conceived the project, LGS and SM designed *Open leaf*. EW performed plant experiments on the system. SL and AB developed the SMART imaging pipeline. LGS, SK and DM worked on data interpretation and visualization. All authors approved the final version of the manuscript.

Data Availability

The data that supports the findings of this study are available in the supplementary material of this article

Table 1 Plant traits measurements extracted using the SMART pipeline.

Measurement	Units	Trait type*	Description
Whole plant area	pixels	WP	Sum of the whole plant area
Whole plant width/height	pixels	WP	The width/height of the plant object, computed from major/minor axis values of the fitted bounding ellipse.
Whole plant solidity	0.00 to 1.00 value range	WP	The ratio of fitted whole plant contour area to its convex hull area, describe the shape of the whole plant, A value of 1 signifies a solid object and a value less than 1 will signify an object having an irregular boundary.
Whole plant curvature	0.00 to 1.00 value range	WP	The derivative of the inclination of the tangent with respect to arc length. The mean curvature value of all leaves, describing the boundary shape change of individual leaf.
Number of leaves	0 to total cluster calculation value range	WP	Count of the total number of leaves
Color distribution	0.00 to 1.00 value range	LS	The distribution and percentage of distinct shades of color on the plant leaf surface.
Leaf area	pixels	LS	Individual leaf area
Leaf width/height	pixels	LS	The width/height of the individual leaf object, computed from major/minor axis values of the fitted bounding ellipse.
Leaf solidity	0.0 to 1.00 value range	LS	The ratio of fitted leaf contour area to its convex hull area.

* WP, whole plant; LS, Leaf specific.

Table 2 Whole rosette area extracted from plants experiencing Fe deficiency.

Time Elapsed (Hours)	Mean ± SD		P Value	Significance
	Replete	-Fe		
0	32.0±2.16	32.0±5.59	0.985	ns
24	26.6±12.9	35.6±7.21	0.282	ns
48	30.3±17.8	48.1±11.8	0.154	ns
72	54.1±16.0	55.4±10.1	0.897	ns
96	72.5±7.11	66.9±8.99	0.373	ns
167	156±17.7	153±22.0	0.83	ns
193	207±30.0	173±23.3	0.134	ns
219	246±30.4	202±31.2	0.0902	ns
241	311±31.9	213±15.9	0.00408	**
267	380±49.4	221±27.8	0.00297	**
297	426±37.3	217±35.7	0.000193	***

Table 2 Welch's t-test was conducted between two groups: replete (5µM Zn 20µM Fe) and the deficient condition -Fe (5µM Zn 0µM Fe) where significance was p-value ≤0.05 (*), ≤0.01(**), ≤001 (***).

Supplementary data

OPEN Leaf Manual (for manual assembly)

STL files (floaters and camera assembly)

Supplementary Table 1 Level of phytohormones in leaves from plants under iron deprivation and MRM transitions for each phytohormone.

Supplementary Table 2 Statistical analyses for all timepoints of whole rosette traits in pixels, average red value, average blue value, and average green value in linear RGB.

Supplementary Table 3 ANOVA results of Figure 6 leaf specific data.

Supplementary Table 4 Rosette traits extracted using SMART.

Supplementary Table 5 Leaf-specific traits extracted using SMART.

References

Acosta-Gamboa L, Liu S, Langley E, Campbell Z, Guerrero N, Mendoza Cozatl D, Lorence A. **2016**. Moderate to severe water limitation differentially affects the phenome and ionome of Arabidopsis. *Functional Plant Biology* **44**.

Awlia M, Nigro A, Fajkus J, Schmoeckel SM, Negrão S, Santelia D, Trtílek M, Tester M, Julkowska MM, Panzarová K. **2016**. High-Throughput Non-destructive Phenotyping of Traits that Contribute to Salinity Tolerance in Arabidopsis thaliana. *Frontiers in Plant Science* **7**: 1414.

Barten PGJ. **1999**. Contrast sensitivity of the human eye and its e ects on image quality. *Storage and Retrieval for Image and Video Databases*.

Billiau K, Sprenger H, Schudoma C, Walther D, Köhl KI. **2012**. Data management pipeline for plant phenotyping in a multisite project. *Functional Plant Biology* **39**: 948–957.

Buckner E, Madison I, Chou H, Matthiadis A, Melvin CE, Sozzani R, Williams C, Long TA. **2019**. Automated Imaging, Tracking, and Analytics Pipeline for Differentiating Environmental Effects on Root Meristematic Cell Division. *Frontiers in Plant Science* **10**: 1487.

Campos ACAL, van Dijk WFA, Ramakrishna P, Giles T, Korte P, Douglas A, Smith P, Salt DE. **2021**. 1,135 ionomes reveal the global pattern of leaf and seed mineral nutrient and trace element diversity in Arabidopsis thaliana. *The Plant Journal* **106**: 536–554.

Chen A, Komives EA, Schroeder JI. **2006**. An Improved Grafting Technique for Mature Arabidopsis Plants Demonstrates Long-Distance Shoot-to-Root Transport of Phytochelatins in Arabidopsis. *Plant Physiology* **141**: 108–120.

Des Marais DL, Hernandez KM, Juenger TE. **2013**. Genotype-by-Environment Interaction and Plasticity: Exploring Genomic Responses of Plants to the Abiotic Environment. *Annual Review of Ecology, Evolution, and Systematics* **44**: 5–29.

Dobrescu A, Scorza LCT, Tsaftaris SA, McCormick AJ. **2017**. A “Do-It-Yourself” phenotyping system: measuring growth and morphology throughout the diel cycle in rosette shaped plants. *Plant Methods* **13**: 95.

Flood PJ, Kruijer W, Schnabel SK, van der Schoor R, Jalink H, Snel JFH, Harbinson J, Aarts MGM. **2016**. Phenomics for photosynthesis, growth and reflectance in Arabidopsis thaliana reveals circadian and long-term fluctuations in heritability. *Plant methods* **12**: 14–14.

García MJ, Romera FJ, Stacey MG, Stacey G, Villar E, Alcántara E, Pérez-Vicente R. **2013**. Shoot to root communication is necessary to control the expression of iron-acquisition genes in Strategy I plants. *Planta* **237**: 65–75.

Hantzis LJ, Kroh GE, Jahn CE, Cantrell M, Peers G, Pilon M, Ravet K. **2018**. A Program for Iron Economy during Deficiency Targets Specific Fe Proteins. *Plant Physiology* **176**: 596–610.

van der Heijden G, Song Y, Horgan G, Polder G, Dieleman A, Bink M, Palloix A, van Eeuwijk F, Glasbey C. **2012**. SPICY: towards automated phenotyping of large pepper plants in the greenhouse. *Functional Plant Biology* **39**: 870–877.

Hernández-Herrera P, Ugartechea-Chirino Y, Torres-Martínez HH, Arzola AV, Chairez-Veloz JE, García-Ponce B, Sánchez M de la P, Garay-Arroyo A, Álvarez-Buylla ER, Dubrovsky JG, *et al.* **2021**. Live Plant Cell Tracking: Fiji plugin to analyze cell proliferation dynamics and understand morphogenesis. *Plant Physiology*: kiab530.

Hindt MN, Guerinot ML. **2012**. Getting a sense for signals: regulation of the plant iron deficiency response. *Biochimica et biophysica acta* **1823**: 1521–1530.

International Commission on Illumination. **2007**. Colorimetry - Part 4: CIE 1976 L*a*b* COLOUR SPACE.

Jackson SA, Iwata A, Lee S-H, Schmutz J, Shoemaker R. **2011**. Sequencing crop genomes: approaches and applications. *The New phytologist* **191**: 915–925.

Khan MA, Castro-Guerrero NA, McInturf SA, Nguyen NT, Dame AN, Wang J, Bindbeutel RK, Joshi T, Jurisson SS, Nusinow DA, *et al.* **2018**. Changes in iron availability in Arabidopsis are rapidly sensed in the leaf vasculature and impaired sensing leads to opposite transcriptional programs in leaves and roots. *Plant, Cell & Environment* **41**: 2263–2276.

Kim SH, Son GH, Bhattacharjee S, Kim HJ, Nam JC, Nguyen PDT, Hong JC, Gassmann W. **2014**. The Arabidopsis immune adaptor SRFR1 interacts with TCP transcription factors that redundantly contribute to effector-triggered immunity. *The Plant Journal* **78**: 978–989.

Le Marié C, Kirchgessner N, Marschall D, Walter A, Hund A. **2014**. Rhizoslides: paper-based growth system for non-destructive, high throughput phenotyping of root development by means of image analysis. *Plant Methods* **10**: 13.

Legris M, Klose C, Burgie ES, Rojas CCR, Neme M, Hiltbrunner A, Wigge PA, Schäfer E, Vierstra RD, Casal JJ. **2016**. Phytochrome B integrates light and temperature signals in Arabidopsis. *Science* **354**: 897.

Lopatkin AJ, Collins JJ. **2020**. Predictive biology: modelling, understanding and harnessing microbial complexity. *Nature Reviews Microbiology* **18**: 507–520.

Lundberg DS, Lebeis SL, Paredes SH, Yourstone S, Gehring J, Malfatti S, Tremblay J, Engelbrektson A, Kunin V, Del Rio TG, *et al.* **2012**. Defining the core Arabidopsis thaliana root microbiome. *Nature* **488**: 86–90.

Maes WH, Steppe K. **2019**. Perspectives for Remote Sensing with Unmanned Aerial Vehicles in Precision Agriculture. *Trends in Plant Science* **24**: 152–164.

Mansencal, Thomas, Mauderer, Michael, Parsons, Michael, Shaw, Nick, Wheatley, Kevin, Cooper, Sean, Vandenberg, Jean D., Canavan, Luke, Crowson, Katherine, Lev, Ofek, *et al.* **2022**. Colour 0.4.2.

Mathieu L, Lobet G, Tocquin P, Périlleux C. **2015**. “Rhizoponics”: a novel hydroponic rhizotron for root system analyses on mature Arabidopsis thaliana plants. *Plant Methods* **11**: 3.

McInturf SA, Khan MA, Gokul A, Castro-Guerrero NA, Höhner R, Li J, Marjault H-B, Fichman Y, Kunz H-H, Goggin FL, *et al.* **2021**. Cadmium interference with iron sensing reveals transcriptional programs sensitive and insensitive to reactive oxygen species. *Journal of Experimental Botany*: erab393.

Moore C, Johnson L, Kwak I-Y, Livny M, Broman K, Spalding E. **2013**. High-Throughput Computer Vision Introduces the Time Axis to a Quantitative Trait Map of a Plant Growth Response. *Genetics* **195**.

Nguyen NT, Khan M, Castro-Guerrero N, Chia J-C, Vatamaniuk O, Mari S, Jurisson S, Mendoza-Cozatl D. **2022**. Iron Availability Within the Leaf Vasculature Determines the Magnitude of Iron Deficiency Responses in Source and Sink Tissues in Arabidopsis. *Plant and Cell Physiology* **63**: 829–841.

Nguyen NT, McInturf SA, Mendoza-Cózatl DG. **2016**. Hydroponics: A Versatile System to Study Nutrient Allocation and Plant Responses to Nutrient Availability and Exposure to Toxic Elements. *Journal of visualized experiments : JoVE*: 54317.

Reynolds D, Baret F, Welcker C, Bostrom A, Ball J, Cellini F, Lorence A, Chawade A, Khafif M, Noshita K, *et al.* **2019**. What is cost-efficient phenotyping? Optimizing costs for different scenarios. *The 4th International Plant Phenotyping Symposium* **282**: 14–22.

Sadeghi-Tehran P, Sabermanesh K, Virlet N, Hawkesford MJ. **2017**. Automated Method to Determine Two Critical Growth Stages of Wheat: Heading and Flowering. *Frontiers in Plant Science* **8**: 252.

Schuler M, Rellán-Álvarez R, Fink-Straube C, Abadía J, Bauer P. **2012**. Nicotianamine functions in the Phloem-based transport of iron to sink organs, in pollen development and pollen tube growth in Arabidopsis. *The Plant cell* **24**: 2380–2400.

Shendure J, Ji H. **2008**. Next-generation DNA sequencing. *Nature Biotechnology* **26**: 1135–1145.

Tsaftaris SA, Scharr H. **2019**. Sharing the Right Data Right: A Symbiosis with Machine Learning. *Trends in Plant Science* **24**: 99–102.

Vasseur F, Bresson J, Wang G, Schwab R, Weigel D. **2018**. Image-based methods for phenotyping growth dynamics and fitness components in Arabidopsis thaliana. *Plant Methods* **14**: 63.

van der Walt S, Schönberger JL, Nunez-Iglesias J, Boulogne F, Warner JD, Yager N, Gouillart E, Yu T, scikit-image contributors. **2014**. scikit-image: image processing in Python. *PeerJ* **2**: e453–e453.

Wang W, Zhang X, Niittylä T. **2019**. OPENER Is a Nuclear Envelope and Mitochondria Localized Protein Required for Cell Cycle Progression in Arabidopsis. *The Plant cell* **31**: 1446–1465.

White JW, Andrade-Sanchez P, Gore MA, Bronson KF, Coffelt TA, Conley MM, Feldmann KA, French AN, Heun JT, Hunsaker DJ, *et al.* 2012. Field-based phenomics for plant genetics research. *Field Crops Research* **133**: 101–112.

Wickham H, Averick M, Bryan J, Chang W, McGowan LD, François R, Grolemund G, Hayes A, Henry L, Hester J, *et al.* 2019. Welcome to the tidyverse. *Journal of Open Source Software* **4**: 1686.

Wild M, Davière J-M, Regnault T, Sakvarelidze-Achard L, Carrera E, Lopez Diaz I, Cayrel A, Dubeaux G, Vert G, Achard P. **2016**. Tissue-Specific Regulation of Gibberellin Signaling Fine-Tunes Arabidopsis Iron-Deficiency Responses. *Developmental Cell* **37**: 190–200.

Wilkinson MD, Dumontier M, Aalbersberg IjJ, Appleton G, Axton M, Baak A, Blomberg N, Boiten J-W, da Silva Santos LB, Bourne PE, *et al.* 2016. The FAIR Guiding Principles for scientific data management and stewardship. *Scientific Data* **3**: 160018.

Xiao Y, Liu H, Wu L, Warburton M, Yan J. **2017**. Genome-wide Association Studies in Maize: Praise and Stargaze. *Molecular plant* **10**: 359–374.

Xie J, Fernandes SB, Mayfield-Jones D, Erice G, Choi M, E Lipka A, Leakey ADB. **2021**. Optical topometry and machine learning to rapidly phenotype stomatal patterning traits for maize QTL mapping. *Plant Physiology* **187**: 1462–1480.

Xu Y. **2016**. Envirotyping for deciphering environmental impacts on crop plants. *Theoretical and Applied Genetics* **129**: 653–673.

Yang W, Feng H, Zhang X, Zhang J, Doonan JH, Batchelor WD, Xiong L, Yan J. **2020**. Crop Phenomics and High-Throughput Phenotyping: Past Decades, Current Challenges, and Future Perspectives. *Molecular Plant* **13**: 187–214.

Yang W, Guo Z, Huang C, Duan L, Chen G, Jiang N, Fang W, Feng H, Xie W, Lian X, *et al.* 2014. Combining high-throughput phenotyping and genome-wide association studies to reveal natural genetic variation in rice. *Nature Communications* **5**: 5087.

Zhang X, Hu Z, Guo Y, Shan X, Li X, Lin J. **2020**. High-efficiency procedure to characterize, segment, and quantify complex multicellularity in raw micrographs in plants. *Plant Methods* **16**: 100.